Supporting Information

CO_2 conversion into methanol under ambient conditions using efficient nanocomposite photocatalyst/solar-energy materials in aqueous medium

Mohsen Lashgari[1, 2*], *Sanaz Soodi*[1]

Lashgari@iasbs.ac.ir

[1]Department of Chemistry, Institute for Advanced Studies in Basic Sciences (IASBS), Zanjan 45137-66731, Iran

[2]Center for Research in Climate Change and Global Warming: Hydrogen and Solar Division, Zanjan 45137-66731, Iran

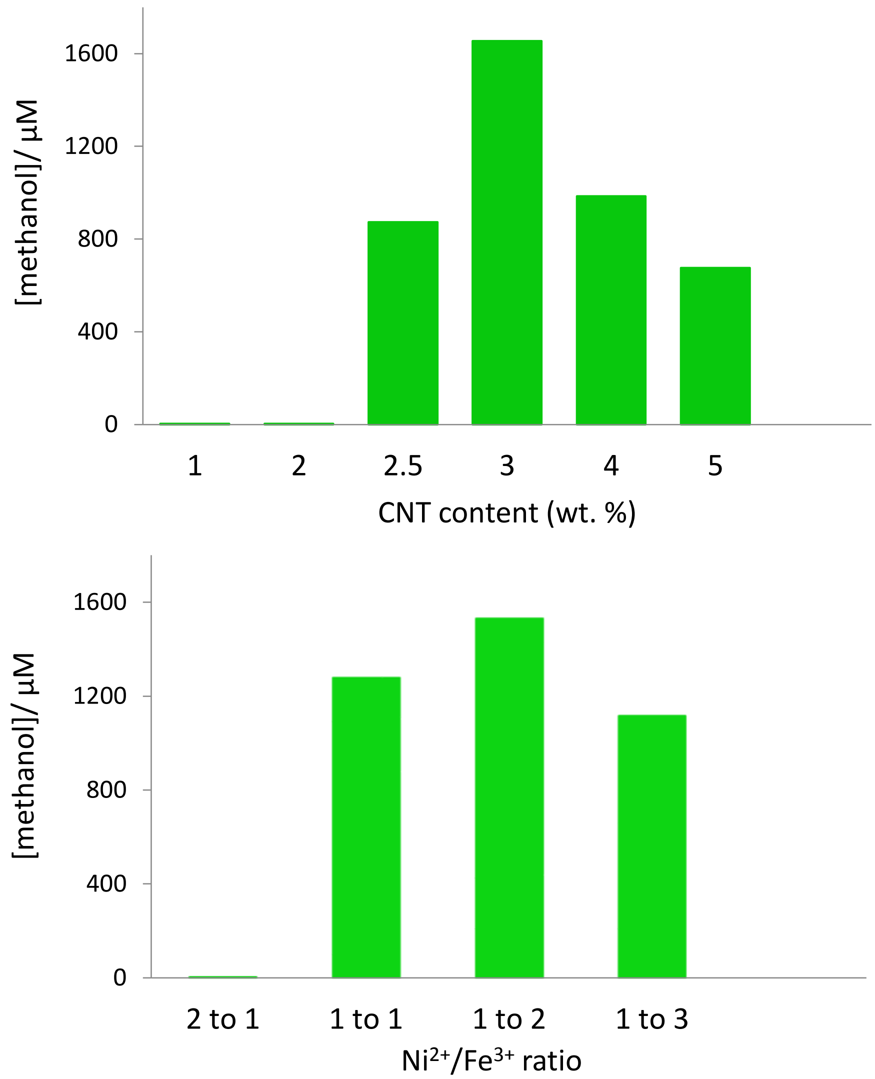

Figure S1: Optimum values of CNT content (3 wt. % of the photocatalyst) and Ni to Fe molar ratio (1:2) for photo-catalytic synthesis of methanol using CO_2 feed in aqueous medium.

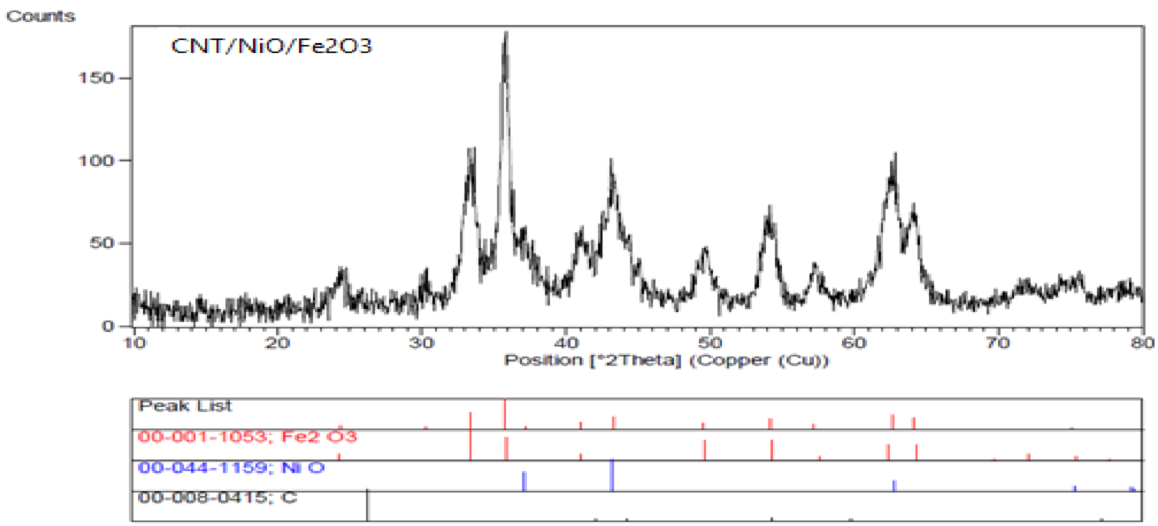
Counts
CNT/NiO/Fe2O3
150
100
50
0
10
20
30
40
50
60
70
80
Position [°2Theta] (Copper (Cu))
Peak List
00-001-1053; Fe2 O3
00-044-1159; Ni O
00-008-0415; C

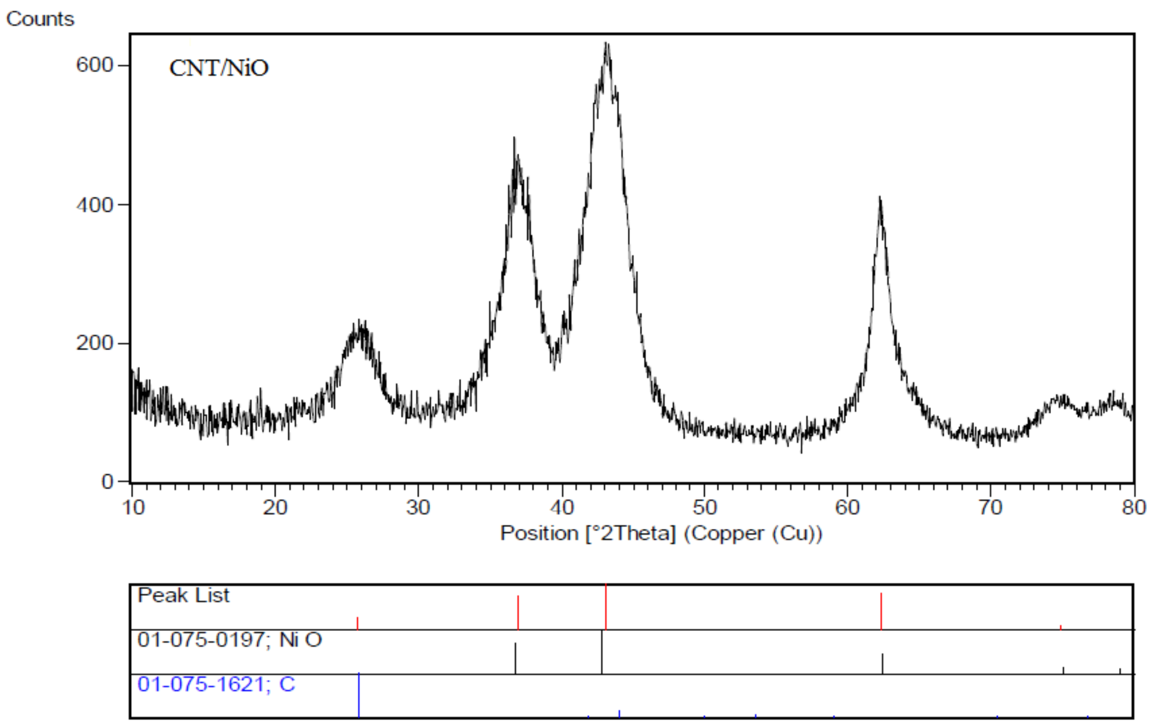
Counts
CNT/NiO
600
400
200
0
10
20
30
40
50
60
70
80
Position [°2Theta] (Copper (Cu))
Peak List
01-075-0197; Ni O
01-075-1621; C

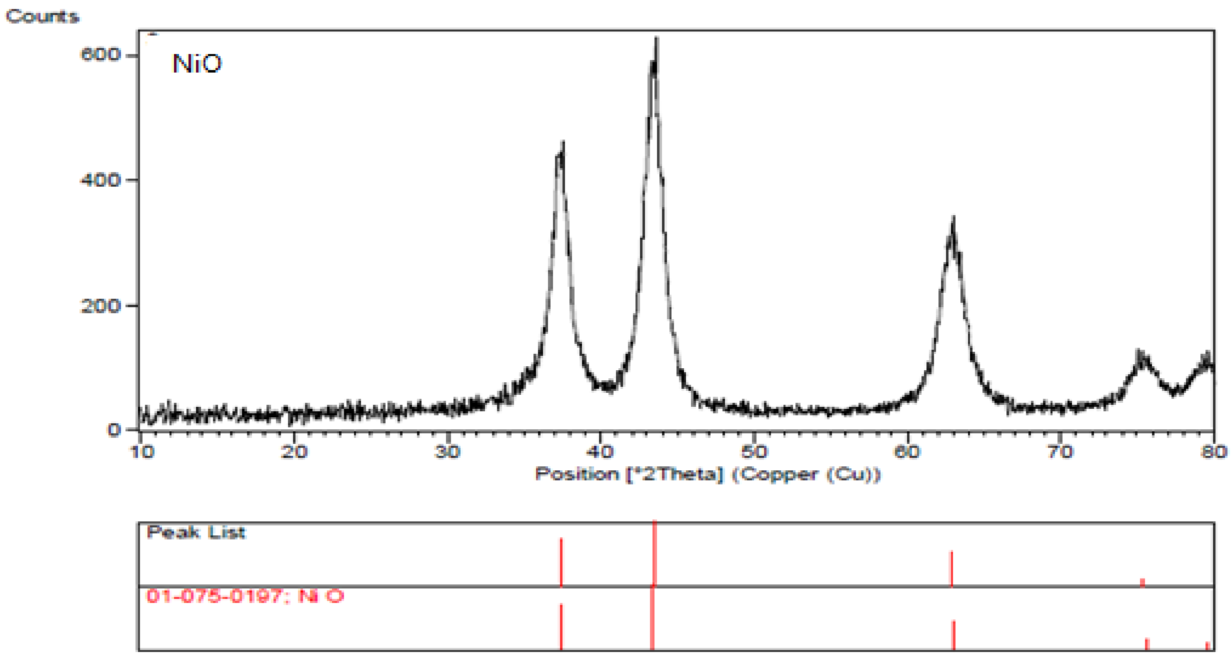
Counts
NiO
600
400
200
0
10
20
30
40
50
60
70
80
Position [°2Theta] (Copper (Cu))
Peak List
01-075-0197; Ni O

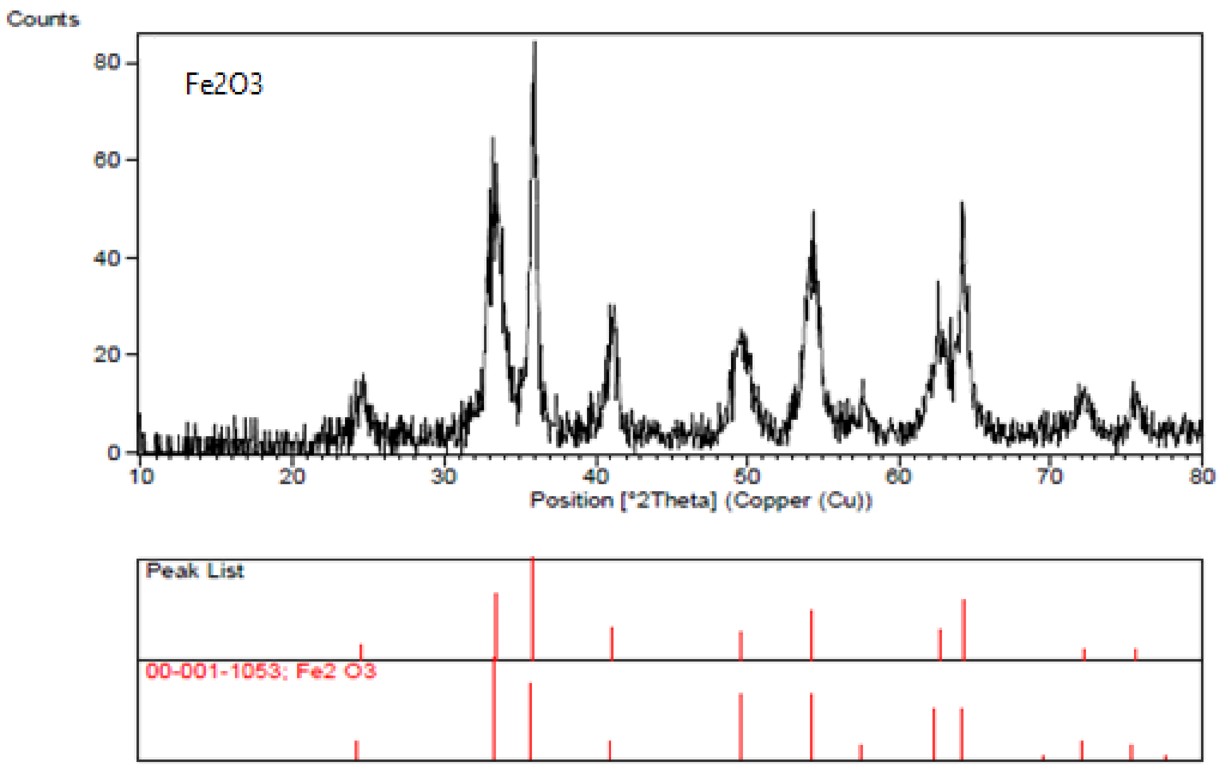
Counts
Fe2O3
80
60
40
20
0
10
20
30
40
50
60
70
80
Position [°2Theta] (Copper (Cu))
Peak List
00-001-1053; Fe2 O3

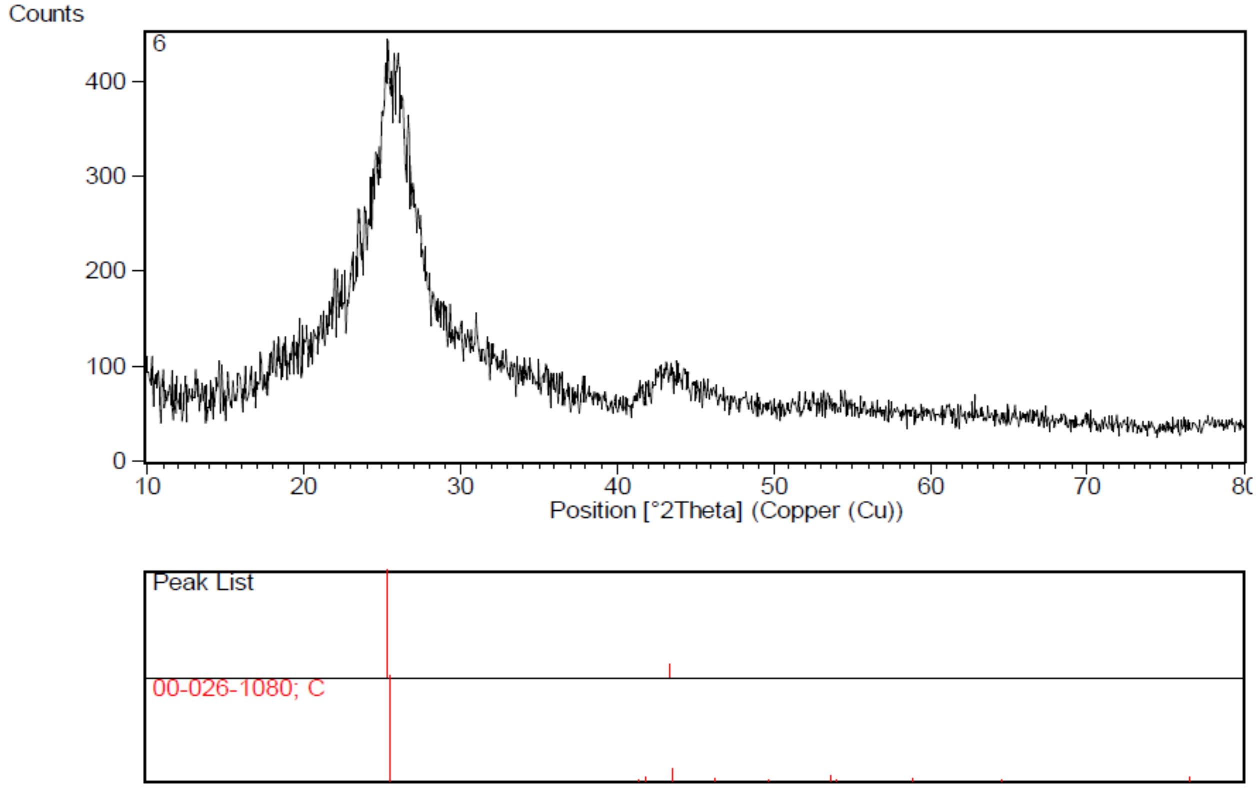

Figure S2. XRD patterns of the composite materials under study, along with their components.

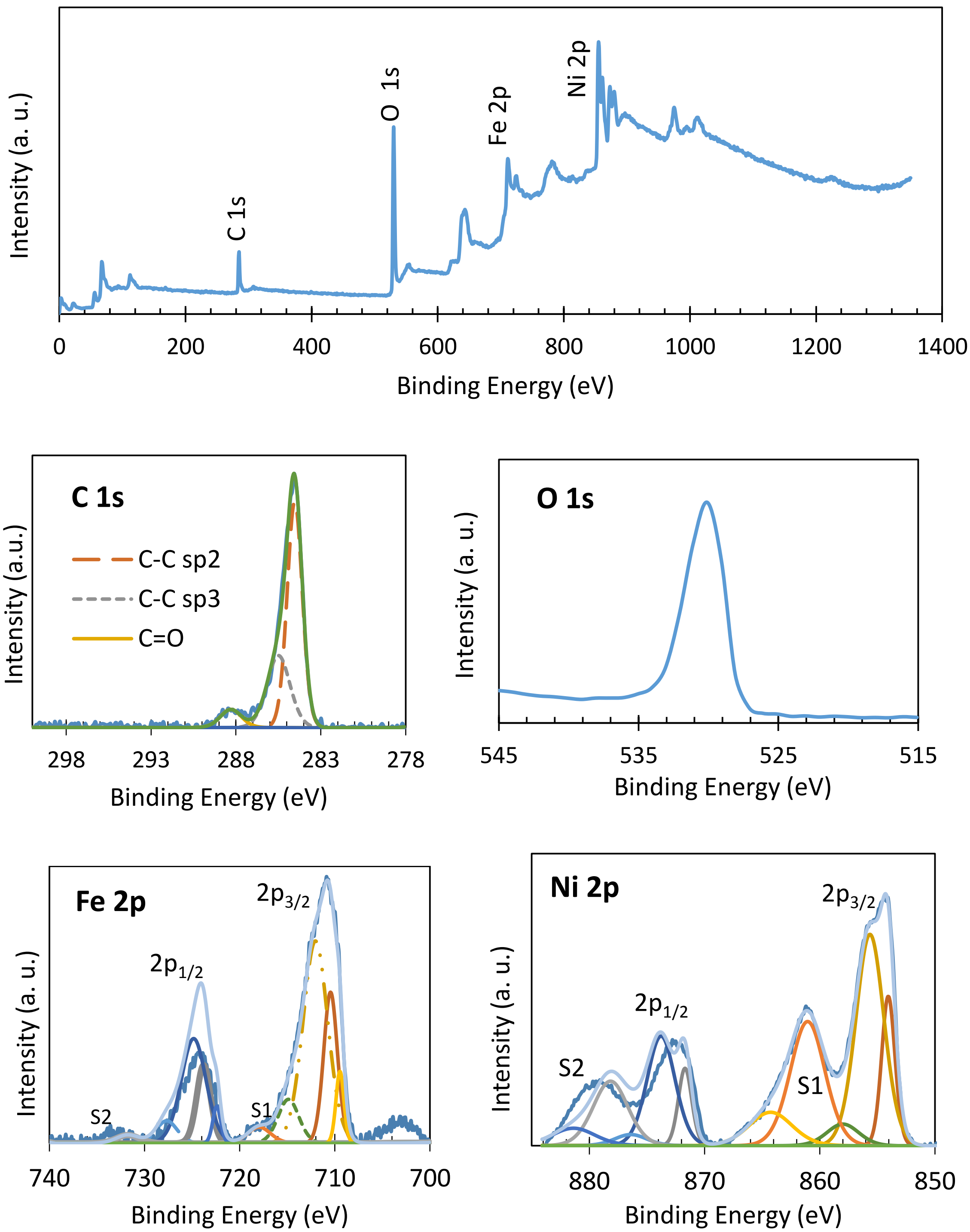

Figure S3. XPS diagram of the composite photocatalyst containing all components (For deconvolution of peaks, a smart background was used and fitting of data were performed with a Lorentzian/Gaussian [LG (30)] line-shape).

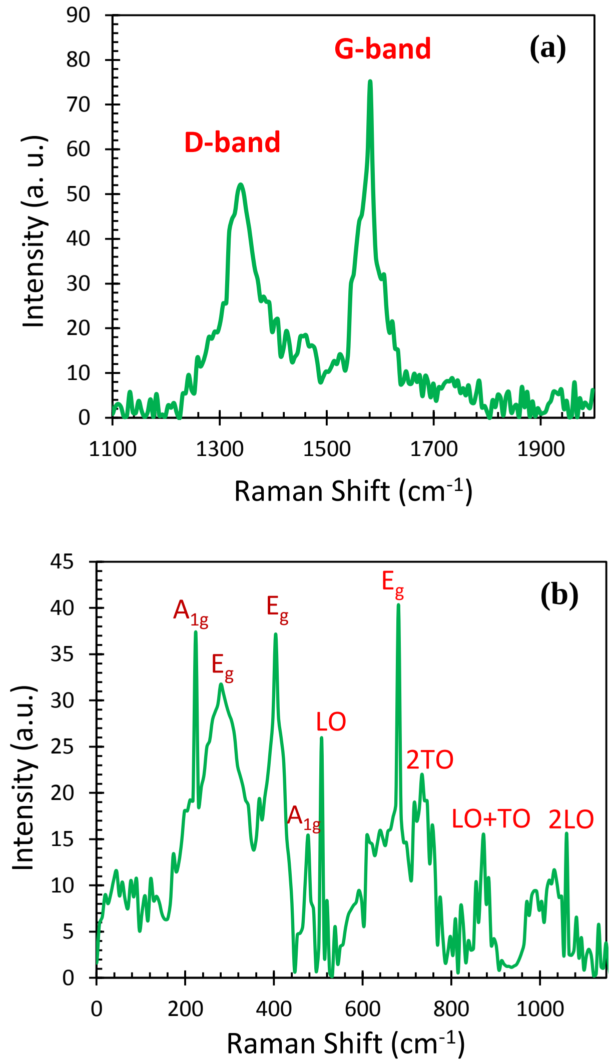

Figure S4. Raman spectrum of the composite photocatalyst containing all components: the spectrum consistes of two parts, 1100-1900 cm^{-1} (a) and 0-1100 cm^{-1} (b), which are related to CNT and NiO/Fe_2O_3 components, respectively.

Here, D and G bands are the characteristic Raman peaks of CNT, verifying its presence in the composite material. The observation of A_{1g} and Eg indicates the formation of Fe_2O_3. The remaining peaks, i.e. LO, 2TO, LO+TO, and 2LO are ascribed to the synthesis of NiO component [Wang et al. Nanoscale Adv. 1, 1200–1206 (2019); Zhang et al. Energy Technol. 6, 263–272 (2018; DOI: 10.1002/ente.201700400); Lu et al. Opt. Express, 19, 16266–16272 (2011); Juma et al. J. Alloys Compd. 723, 866–872 (2017).].

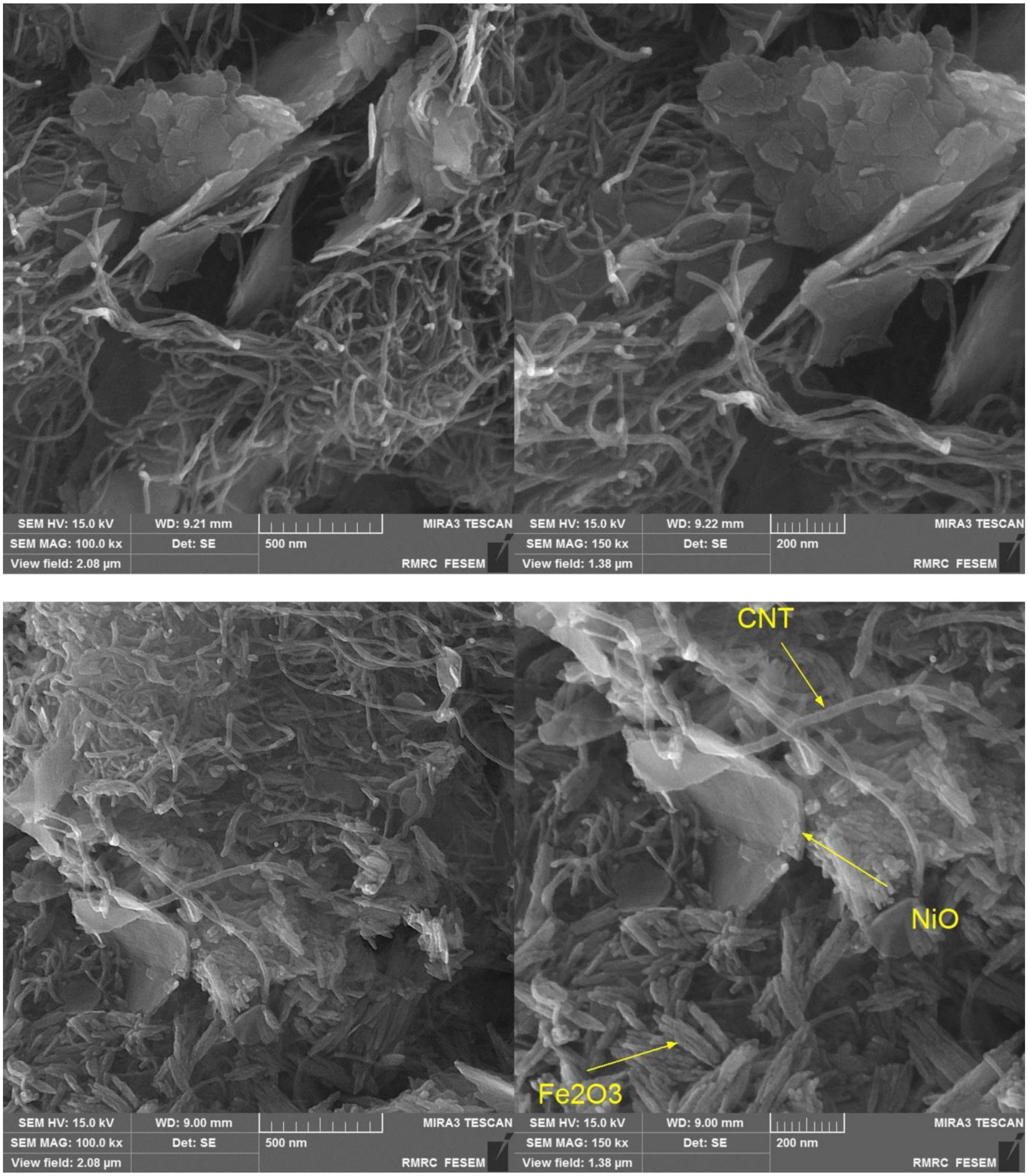

Figure S5: Extra SEM images taken at higher magnification for the binary (first row; CNT/NiO) and ternary (second row; CNT/NiO/Fe_2O_3) composite photocatalysts.

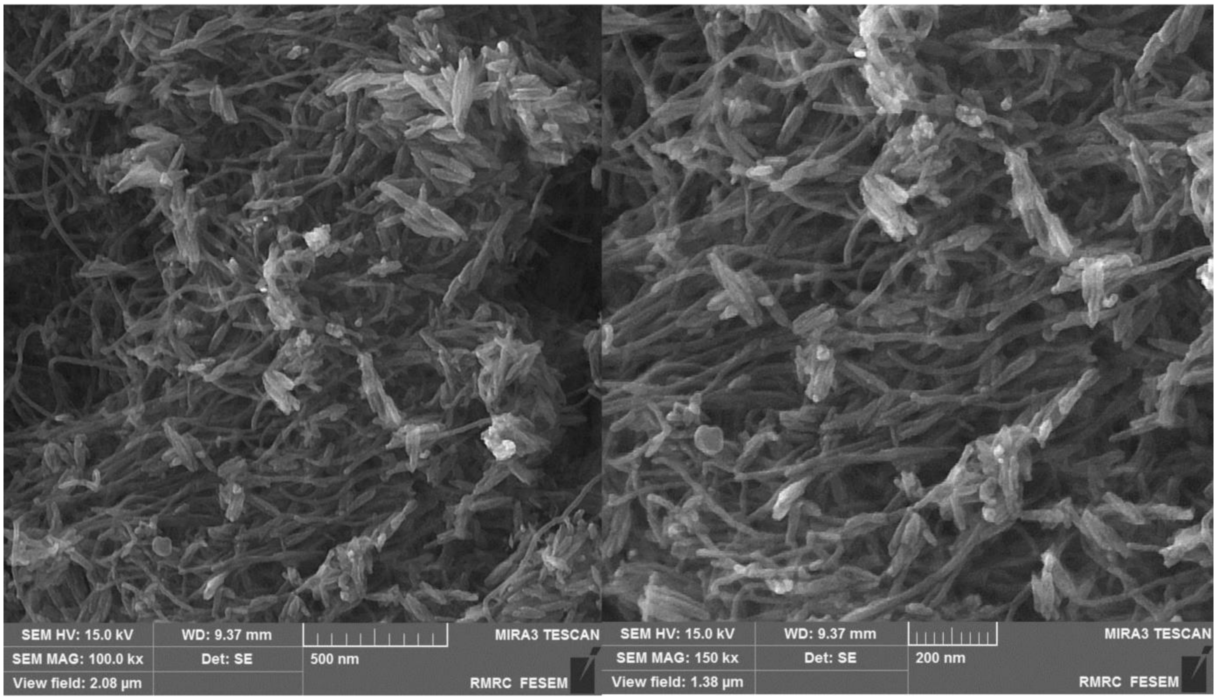

Figure S6: Extra SEM evidence for nano-rod morphology due to Fe_2O_3 presence in the composite photocatalyst. The images were taken at two different magnifications from the ternary photocatalyst synthesized in the absence of NiO, i.e. CNT/Fe_2O_3.

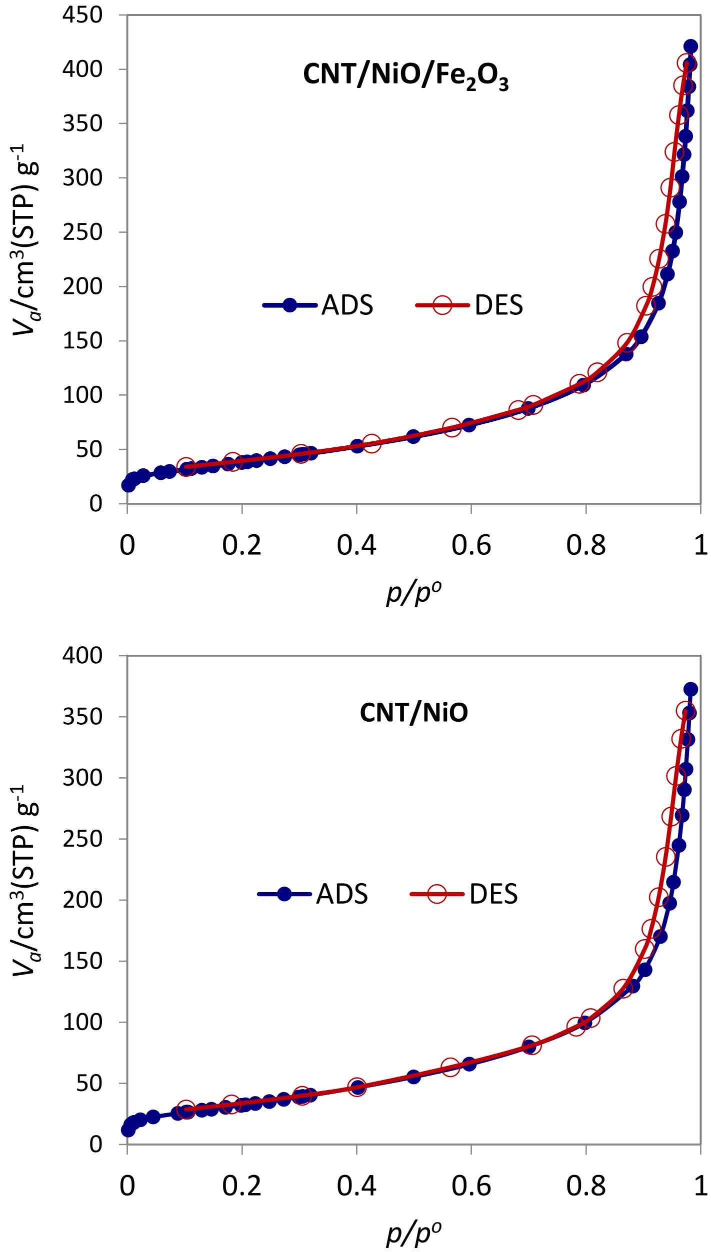

Figure S7: Nitrogen adsorption-desorption plots of the composite photocatalysts.

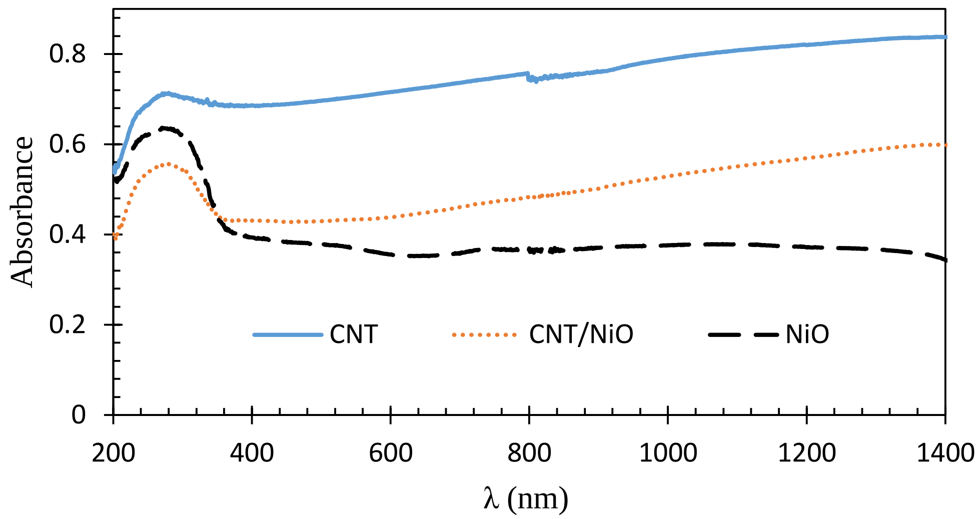

Figure S8: Diffuse reflectance spectra of CNT, NiO and CNT/NiO, depicted in a wide UV-Vis-NIR spectral region.

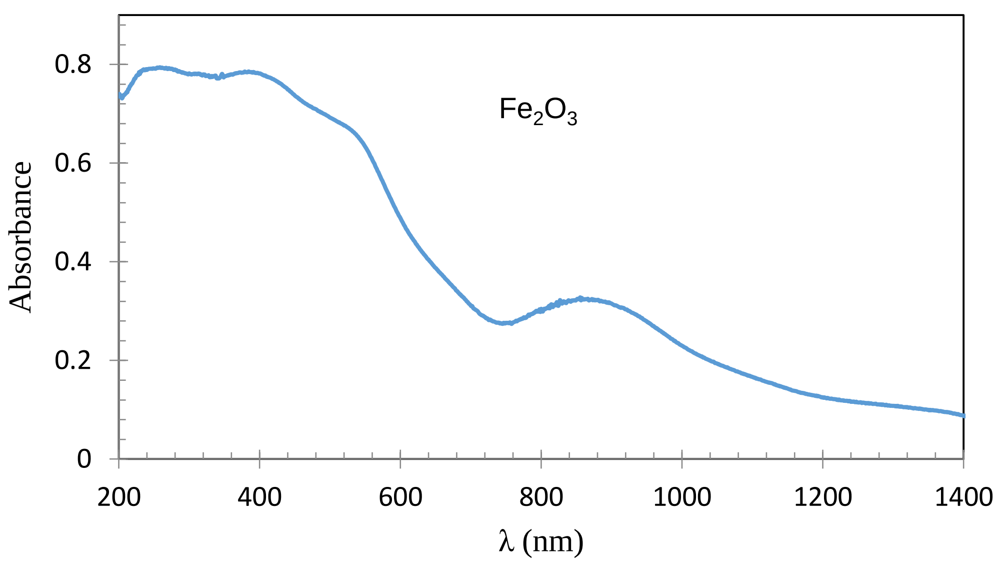

Figure S9: Diffuse reflectance spectrum of Fe_2O_3.

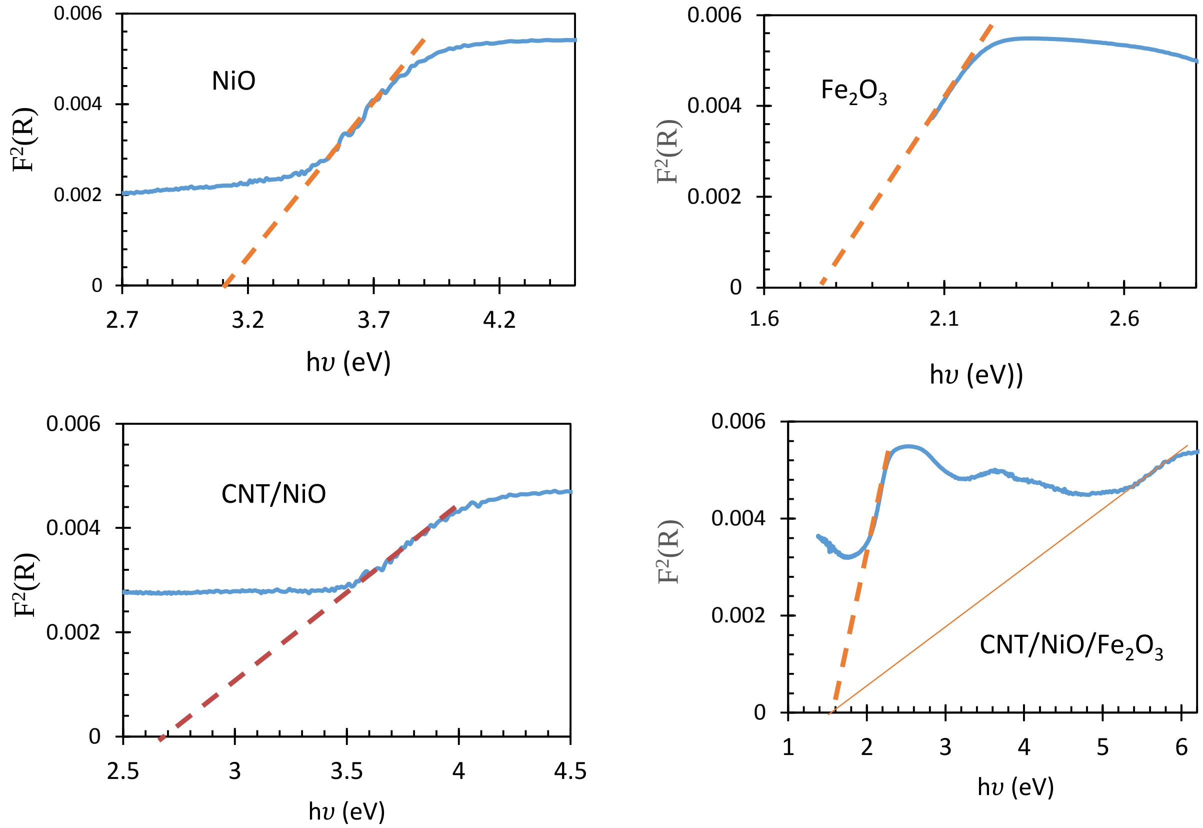

Figure S10: Bandgap of the photocatalyst/solar-energy materials, determined through the Kubelka-Munk approach [F(R) is defined as $(1\text{-}R)^2/2R$ and R is reflectance; for more details, see references 22 and 26 of the main text].

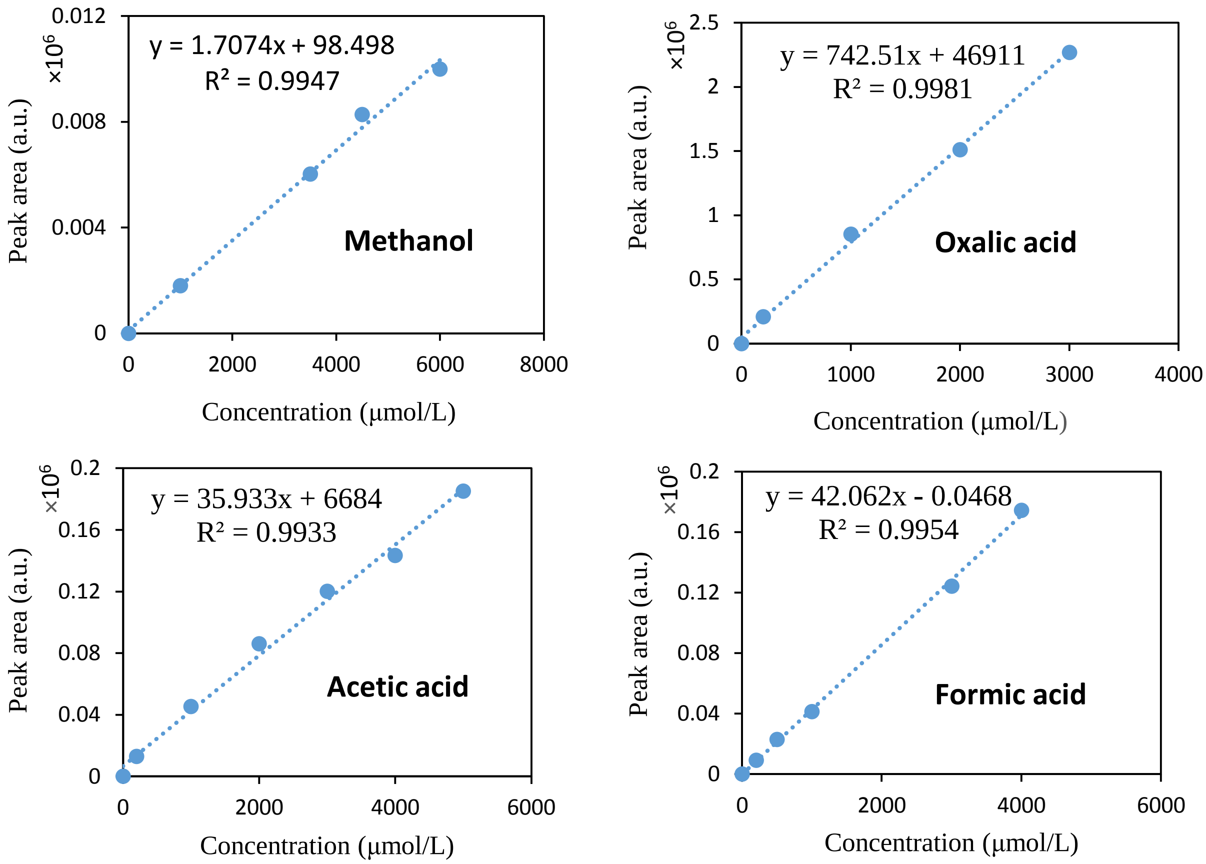

Figure S11: Calibration diagrams of methanol, oxalic acid, acetic acid and formic acid aqueous solutions determined through HPLC analysis.

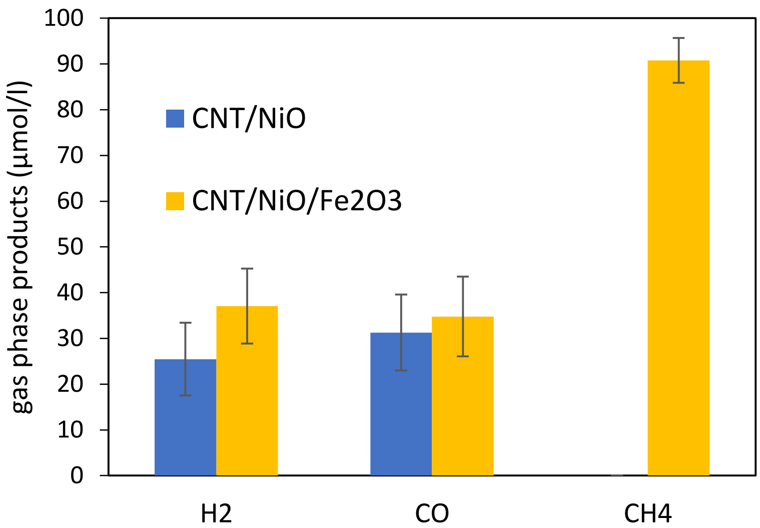

Figure S12: Non-liquid [gas phase] products (hydrogen, carbon monoxide and methane) generated during the CO_2 photoconversion process upon the binary and ternary photocatalysts [data were obtained using an online gas chromatograph (GC, SRI instruments 8610C) equipped with TCD and FID detectors connected to the reactor outlet].

No methane was detected for CNT/NiO, suggesting the lack of methyl formation, which is crucial in the synthesis of methane [Schouten et al, Chem. Sci., 2011, 2, 1902]. This evidence indicates by preventing the methane (methyl) formation, why the extent of methanol decreases for the binary photocatalyst [here, the only route for methanol production is $CH_3\dot{O}/\dot{H}$ reaction not $\dot{C}H_3/\dot{O}H$ one; see **eq. 7** of the main text]. On the contrary, in the case of CNT/NiO/Fe_2O_3, both reaction pathways are available for the synthesis of methanol, and CH_4 (the result of $\dot{C}H_3/\dot{H}$ recombination) is the major gas-phase product.

Table S1. A comparison between this work and related studies reported for photocatalytic synthesis of methanol using CO_2 feed in aqueous media.

Photocatalyst	Methanol yield	Explanation	Ref.
CNT/NiO/Fe_2O_3 (50 mg in 50 ml H_2O)	4382 (µmol/l)	500 W Xenon Intensity: 100 mW.cm^{-2}, 2 h illumination	This work
CNT/NiO (50 mg in 50 ml H_2O)	1655 (µmol/l)	"	"
NiO/$K_2Ta_2O_6$ (20 mg in 20 ml H_2O)	1815 (µmol/l.g.h)	250 W Mercury lamp (wavelength: 365 nm)	[1]
CeO_2/Bi_2MoO_z 50 mg in 50ml H_2O	32.5 (µmol/g)	300 W Xenon 420 nm cut-off filter 5 cm above the reactor, 4 h illumination	[2]
rGO/$InVO_4$/Fe_2O_3 DMF/H_2O/Et_3N (3:1:1)	16.9 (mmol/g)	20 W LED Intensity: not mentioned, 24 h illumination	[3]
***o*-$BiVO_4$** 0.2g in 160ml H_2O	398.3 (µmol/g.hr)	300 W Xenon Intensity: 100 mW.cm^{-2}	[4]
TiO_2 nanocrystals 0.05g in 30ml H_2O	2.5 (µmol/g)	500 W high-pressure Xenon Intensity: 2.5 mW.cm^{-2} UV and 0.12 mW cm^{-2} visible light, 10 h illumination	[5]
CoPc-Rs/Fe_2O_3 NTs Composite film on Fe sheet, in 0.1 M $KHCO_3$	138 (µmol L^{-1} cm^{-2})	Visible light irradiation Intensity: not mentioned, 6.5 h illumination under cathodic bias (−1.3 V_{SCE}; photoelectrochemical)	[6]
Fe_2O_3-TiO_2 (2 g/L in the presence of sulfite hole scavenger)	319.42 (µmol/g)	250 W Mercury lamp of UV high pressure Intensity: not mentioned, 7 h illumination at 90 ℃	[7]
SnO_2/Fe_2O_3 Photocatalyst film in 0.1M $KHCO_3$	0.69 (mmol L^{-1} cm^{-2})	Xenon lamp with a band-pass filter (λ= 420 nm, 100 mW.cm^{-2}), 6 h illumination	[8]
MoS_2–TiO_2 (0.1 g in 200 mL of 1 M $NaHCO_3$)	10.6 (µmol/g.hr)	300 W xenon Intensity: not mentioned	[9]

Ni/$InTaO_4$ 0.02 g in 20 ml solution of acetonitrile, water and TEOA (3:1:1)	200 (µmol/g)	20 W white LED, 5 cm distance, 70 h illumination	[10]
In_2O_3-WO_3 (details: not mentioned)	496 (µmol/g.hr)	355 high power laser beam, 1.5 cm distance	[11]
rGO/ $SrTi_{0.95}Fe_{0.05}O_{3-\delta}$ 50 mg in 50 mL of RhB (10^{-5} M) and NaOH (0.02M).	24.07 (µmol/g.hr)	300 W Xenon (320 nm≤ λ≥ 780 nm) Intensity: 160 $mW.cm^{-2}$	[12]
g-C_3N_4/(Cu/TiO_2) 0.2 g in 400 ml 1M NaOH	2500 (µmol/g)	254 nm UV light, 8 h illumination Intensity: 5.4 $mW.cm^{-2}$	[13]
$CdIn_2S_4$/ g-C_3N_4 0.1 g in 100 ml 0.1M NaOH solution	31 (µmol/g.hr)	300W Xenon with a UV cut-off filter (λ>420nm) Intensity: 15 $mW.cm^{-2}$	[14]
Bi_2WO_6 0.2 g in 100 ml H_2O	23 (µmol/g)	300 W Xenon Intensity: not mentioned	[15]
Bi_2S_3 20 mg in 80 ml H_2O	320.2 (µmol/g)	300W Xenon with a UV cut-off filter (λ>420nm), 5 cm above the cell	[16]
Bi_2MoO_6 50 mg in 50 ml H_2O	24.8 (µmol/g)	300 W Xenon Intensity: not mentioned	[17]
WO_3 (details: not mentioned)	9.77 (µmol/g)	300W Xenon with a UV cut-off filter (λ>420nm) Intensity: not mentioned	[18]
GrO/CuO 100 mg in 50 ml solution (DMF and H_2O)	1282 (µmol/g)	20 W white cold LED Intensity: 85 W/m^2, 24 h illumination	[19]
CQD/Cu_2O 35 mg in 20 ml H_2O	55.7 (µmol/g.h)	300 W Xenon Intensity: not mentioned	[20]
GO-$(TBA)_2Mo_6Br^i_8Br^a_x$ 100mg in 50 ml solution (10 ml H_2O and 40 ml DMF)	1644 (µmol/g)	20 W white cold LED Intensity: 75 W/m^2	[21]

g-C_3N_4/ZnO 100 mg in H_2O vapor, 0.12 g $NaHCO_3$, 0.25 ml HCl 4M	0.6 (µmol/g.h)	300 W Xenon 10 cm apart (vertically positioned above the reactor chamber)	[22]
Cu/TiO_2 NFF photocatalyst film in 100 ml H_2O	1.8 (µmol/cm^2 h)	500W Xenon lamp with a 420 nm cut-off filter Intensity: not mentioned	[23]
Bi_2S_3/CeO_2 10 mg in 100 ml H_2O	1346.8 (µmol/g)	300 W Xenon Intensity: 1.3 W 8 h illumination	[24]
Si/TiO_2 4.2 cm^2 in 0.4 ml DW	197 µM	300 W Xenon 150 min illumination Intensity: not mentioned	[25]
Gr/TiO_2 0.05 g in 50ml $NaHCO_3$ (0.08 M)	0.680 (µmol /g.h)	500 W Xenon Intensity: not mentioned	[26]
3% NiO_x–Ta_2O_5 0.2 g in 10 ml H_2O	50 (µmol)	400 W Halogen lamp Intensity: not mentioned	[27]
Lamellar $BiVO_4$ 0.2 g in 100 ml H_2O	30 (µmol)	300 W Xenon Intensity: not mentioned	[28]
RuO_2-modified $Cu_xAg_yIn_zZn_kS_m$ 0.05 g in 50 ml H_2O	118.5 (µmol/g.h)	1000 W Xenon Intensity: not mentioned	[29]
Ni/NiO-loaded N-$InTaO_4$ 0.1 g in 50 ml H_2O	350 (µmol/g)	Xenon lamp Intensity: 100 mW	[30]
NiO/$InTaO_4$ 0.14 g in 50ml H_2O	1.3 (µmol.l^{-1}.h^{-1}.g^{-1})	500 W Halogen lamp Intensity: not mentioned	[31]

References:

[1] Shao, X., Yin, X. and Wang, J., 2018. Nanoheterostructures of potassium tantalate and nickel oxide for photocatalytic reduction of carbon dioxide to methanol in isopropanol. *Journal of colloid and interface science*, *512*, pp.466-473.

[2] Dai, W., Hu, X., Wang, T., Xiong, W., Luo, X. and Zou, J., 2018. Hierarchical CeO_2/Bi_2MoO_6 heterostructured nanocomposites for photoreduction of CO_2 into hydrocarbons under visible light irradiation. *Applied Surface Science*, *434*, pp.481-491.

[3] Kumar, A., Prajapati, P.K., Pal, U. and Jain, S.L., 2018. Ternary $rGO/InVO_4/Fe_2O_3$ Z-scheme heterostructured photocatalyst for CO_2 reduction under visible light irradiation. *ACS Sustainable Chemistry & Engineering*, *6*, pp.8201-8211.

[4] Gao, S., Gu, B., Jiao, X., Sun, Y., Zu, X., Yang, F., Zhu, W., Wang, C., Feng, Z., Ye, B. and Xie, Y., 2017. Highly efficient and exceptionally durable CO_2 photoreduction to methanol over freestanding defective single-unit-cell bismuth vanadate layers. *Journal of the American Chemical Society*, *139*, pp.3438-3445.

[5] Truong, Q.D., Hoa, H.T., Vo, D.V.N. and Le, T.S., 2017. Controlling the shape of anatase nanocrystals for enhanced photocatalytic reduction of CO_2 to methanol. *New Journal of Chemistry*, *41*, pp.5660-5668.

[6] Yang, Z., Xu, J., Wu, C., Jing, H., Li, P., Yin, H., 2014. New insight into photoelectric converting CO_2 to CH_3OH on the one-dimensional ribbon CoPc enhanced Fe_2O_3 NTs. *Applied Catalysis B: Environmental* 156-157, pp. 249-256.

[7] Wang, J., Liu, H., Xu, Y., Zhang, X., 2014. Preparation of Fe_2O_3-TiO_2 and its photocatalytic reduction of CO_2 to methanol. *Asian Journal of Chemistry* 26, pp. 3875-3878.

[8] Yang, Z., Wang, H., Song, W., Wei, W., Mu, Q., Kong, B., Li, P. and Yin, H., 2017. One dimensional SnO_2 NRs/Fe_2O_3 NTs with dual synergistic effects for photoelectrocatalytic reduction CO_2 into methanol. *Journal of Colloid and Interface Science*, *486*, pp.232-240.

[9] Tu, W., Li, Y., Kuai, L., Zhou, Y., Xu, Q., Li, H., Wang, X., Xiao, M. and Zou, Z., 2017. Construction of unique two-dimensional MoS_2–TiO_2 hybrid nanojunctions: MoS_2 as a promising cost-effective cocatalyst toward improved photocatalytic reduction of CO_2 to methanol. *Nanoscale*, *9*(26), pp.9065-9070.

[10] Singhal, N., Goyal, R. and Kumar, U., 2017. Visible-light-assisted photocatalytic CO_2 reduction over $InTaO_4$: selective methanol formation. *Energy & Fuels*, *31*(11), pp.12434-12438.

[11] Gondal, M.A., Dastageer, M.A., Oloore, L.E. and Baig, U., 2017. Laser induced selective photo-catalytic reduction of CO_2 into methanol using In_2O_3-WO_3 nano-composite. *Journal of Photochemistry and Photobiology A: Chemistry*, *343*, pp.40-50.

[12] Dong, W.H., Wu, D.D., Luo, J.M., Xing, Q.J., Liu, H., Zou, J.P., Luo, X.B., Min, X.B., Liu, H.L., Luo, S.L. and Au, C.T., 2017. Coupling of photodegradation of RhB with photoreduction of CO_2 over rGO/$SrTi_{0.95}Fe_{0.05}O_{3-\delta}$ catalyst: A strategy for one-pot conversion of organic pollutants to methanol and ethanol. *Journal of Catalysis*, *349*, pp.218-225.

[13] Adekoya, D.O., Tahir, M. and Amin, N.A.S., 2017. g-C_3N_4/(Cu/TiO_2) nanocomposite for enhanced photoreduction of CO_2 to CH_3OH and HCOOH under UV/visible light. *Journal of CO_2 Utilization*, *18*, pp.261-274.

[14] Liu, H., Zhang, Z., Meng, J. and Zhang, J., 2017. Novel visible-light-driven CdIn2S4/mesoporous g-C_3N_4 hybrids for efficient photocatalytic reduction of CO_2 to methanol. *Molecular Catalysis*, *430*, pp.9-19.

[15] Jiang, Z., Liang, X., Zheng, H., Liu, Y., Wang, Z., Wang, P., Zhang, X., Qin, X., Dai, Y., Whangbo, M.H. and Huang, B., 2017. Photocatalytic reduction of CO_2 to methanol by three-dimensional hollow structures of Bi_2WO_6 quantum dots. *Applied Catalysis B: Environmental*, *219*, pp.209-215.

[16] Jin, J. and He, T., 2017. Facile synthesis of Bi_2S_3 nanoribbons for photocatalytic reduction of CO_2 into CH_3OH. *Applied Surface Science*, *394*, pp.364-370.

[17] Dai, W., Yu, J., Xu, H., Hu, X., Luo, X., Yang, L. and Tu, X., 2016. Synthesis of hierarchical flower-like Bi_2MoO_6 microspheres as efficient photocatalyst for photoreduction of CO_2 into solar fuels under visible light. *CrystEngComm*, *18*(19), pp.3472-3480.

[18] Wang, L., Wang, Y., Cheng, Y., Liu, Z., Guo, Q., Ha, M.N. and Zhao, Z., 2016. Hydrogen-treated mesoporous WO_3 as a reducing agent of CO_2 to fuels (CH_4 and CH_3OH) with enhanced photothermal catalytic performance. *Journal of Materials Chemistry A*, *4*, pp.5314-5322.

[19] Gusain, R., Kumar, P., Sharma, O.P., Jain, S.L. and Khatri, O.P., 2016. Reduced graphene oxide–CuO nanocomposites for photocatalytic conversion of CO_2 into methanol under visible light irradiation. *Applied Catalysis B: Environmental*, *181*, pp.352-362.

[20] Li, H., Zhang, X. and MacFarlane, D.R., 2015. Carbon quantum dots/Cu_2O heterostructures for solar-light-driven conversion of CO_2 to methanol. *Advanced Energy Materials*, *5*(5), p.1401077.

[21] Kumar, P., Mungse, H.P., Cordier, S., Boukherroub, R., Khatri, O.P. and Jain, S.L., 2015. Hexamolybdenum clusters supported on graphene oxide: Visible-light induced photocatalytic reduction of carbon dioxide into methanol. *Carbon*, *94*, pp.91-100.

[22] Yu, W., Xu, D. and Peng, T., 2015. Enhanced photocatalytic activity of g-C_3N_4 for selective CO_2 reduction to CH_3OH via facile coupling of ZnO: a direct Z-scheme mechanism. *Journal of Materials Chemistry A*, *3*, pp.19936-19947.

[23] Liu, E., Qi, L., Bian, J., Chen, Y., Hu, X., Fan, J., Liu, H., Zhu, C. and Wang, Q., 2015. A facile strategy to fabricate plasmonic Cu modified TiO_2 nano-flower films for photocatalytic reduction of CO_2 to methanol. *Materials Research Bulletin*, *68*, pp.203-209.

[24] Ijaz, S., Ehsan, M.F., Ashiq, M.N. and He, T., 2015. Synthesis of a Bi_2S_3/CeO_2 nanocatalyst and its visible light-driven conversion of CO_2 into CH_3OH and CH_4. *Catalysis Science & Technology*, *5*(12), pp.5208-5215.

[25] Liu, Y., Ji, G., Dastageer, M.A., Zhu, L., Wang, J., Zhang, B., Chang, X. and Gondal, M.A., 2014. Highly-active direct Z-scheme Si/TiO_2 photocatalyst for boosted CO_2 reduction into value-added methanol. *RSC Advances*, *4*, pp.56961-56969.

[26] Baeissa, E.S., 2014. Green synthesis of methanol by photocatalytic reduction of CO_2 under visible light using a graphene and tourmaline co-doped titania nanocomposites. *Ceramics International*, *40*(8), pp.12431-12438.

[27] Lv, X.J., Fu, W.F., Hu, C.Y., Chen, Y. and Zhou, W.B., 2013. Photocatalytic reduction of CO_2 with H_2O over a graphene-modified NiO_x–Ta_2O_5 composite photocatalyst: coupling yields of methanol and hydrogen. *RSC Advances*, *3*, pp.1753-1757.

[28] Mao, J., Peng, T., Zhang, X., Li, K. and Zan, L., 2012. Selective methanol production from photocatalytic reduction of CO_2 on $BiVO_4$ under visible light irradiation. *Catalysis Communications*, *28*, pp.38-41.

[29] Liu, J.Y., Garg, B. and Ling, Y.C., 2011. $Cu_xAg_yIn_zZn_kS_m$ solid solutions customized with RuO_2 or $Rh_{1.32}Cr_{0.66}O_3$ co-catalyst display visible light-driven catalytic activity for CO_2 reduction to CH_3OH. *Green Chemistry*, *13*(8), pp.2029-2031.

[30] Tsai, C.W., Chen, H.M., Liu, R.S., Asakura, K. and Chan, T.S., 2011. Ni@NiO core–shell structure-modified nitrogen-doped $InTaO_4$ for solar-driven highly efficient CO_2 reduction to methanol. *The Journal of Physical Chemistry C*, *115*, pp.10180-10186.

[31] Pan, P.W. and Chen, Y.W., 2007. Photocatalytic reduction of carbon dioxide on $NiO/InTaO_4$ under visible light irradiation. *Catalysis Communications*, *8*, pp.1546-1549.